Finite-size effects on the hadron-quark phase transition in neutron stars

X. H. Wu and H. Shen*
School of Physics, Nankai University, Tianjin 300071, China
(Received 16 May 2017; published 14 August 2017)

We study the finite-size effects, like the surface and Coulomb energies, on the hadron-quark mixed phase in neutron stars. The equilibrium conditions for coexisting hadronic and quark phases are derived by minimizing the total energy including the surface and Coulomb contributions, which are different from the Gibbs conditions without finite-size effects. We employ the relativistic mean-field model to describe the hadronic phase, while the Nambu-Jona-Lasinio model with vector interactions is used for the quark phase. It is found that finite-size effects can significantly reduce the region of the mixed phase, and the results lie between those of the Gibbs and Maxwell constructions. We show that a massive star may contain a mixed phase core and its size depends on the surface tension of the hadron-quark interface and the vector coupling between quarks. The repulsive vector interaction in the Nambu-Jona-Lasinio model can stiffen the equation of state of quark matter, and therefore delay the phase transition and increase the maximum mass of neutron stars.

DOI: 10.1103/PhysRevC.96.025802

I. INTRODUCTION

Neutron stars provide a unique environment for the study of cold and dense matter. It is expected that the phase transition from hadronic matter to quark matter may occur in the core of massive neutron stars [1–3]. Over the past decades, many authors have studied the deconfinement phase transition of neutron-star matter and its influence on properties of neutron stars [4–14]. Most of these studies are based on the bulk approximation, in which the hadron-quark phase transition is performed through the Maxwell or Gibbs constructions. In the Maxwell construction, local charge neutrality is imposed, while the coexisting hadronic and quark phases have equal pressure and baryon chemical potential but different electron chemical potential. The pressure of the mixed phase in the Maxwell construction remains constant, and therefore such a mixed phase is not allowed to appear inside neutron stars. With the Gibbs conditions for phase equilibrium, only global charge neutrality is required, while hadronic and quark phases have opposite electric charges. The mixed phase in the Gibbs construction persists over a finite range of pressure, so it is possible for the massive neutron star to contain a mixed-phase region in its interior. It has been shown in Ref. [15] that there are significant differences in the behavior of compact stars between Maxwell and Gibbs constructions.

In general, the mixed phase with the Gibbs construction is energetically more favorable than the one with the Maxwell construction. However, when the surface and Coulomb energies are taken into account, the energy density of the quark-droplet phase may be higher than that of the Maxwell construction due to a large surface tension [16]. A detailed calculation including charge screening indicates that the mixed phase with a large surface tension behaves like that of the Maxwell construction, while the one with a small surface tension is close to the case of the Gibbs construction [17–19]. In fact, the Maxwell and Gibbs constructions correspond to the two limits of infinite and zero surface tension, respectively. It is interesting to examine the effect of a finite surface tension on properties of the hadron-quark mixed phase.

In an earlier study performed by Heiselberg *et al.* [16], the Coulomb and surface effects were examined for the description of the hadron-quark mixed phase. The geometrical structure and size of the mixed phase could be determined by competition between surface and Coulomb energies. The possible geometrical structure of the mixed phase has been extensively discussed in Refs. [17–21], which may change from droplet to rod, slab, tube, and bubble with increasing density. It was reported in Refs. [17,22] that the charge screening effect and the rearrangement of charged particles should be taken into account for a realistic description of the hadron-quark mixed phase. In most of the studies on the finite-size effects, the coexisting hadronic and quark phases were required to satisfy the Gibbs conditions for phase equilibrium. An additional pressure due to the surface tension was also included in the pressure equilibrium condition [17]. In fact, the equilibrium conditions would be modified when the surface and Coulomb energies are taken into account. Proper equilibrium conditions could be derived by minimizing the total free energy of a system [23,24]. It is important to examine the equilibrium conditions between the hadronic and quark phases with inclusion of the surface and Coulomb terms.

In the present work, we employ the Wigner-Seitz approximation to describe the hadron-quark mixed phase. We derive the equilibrium conditions for coexisting hadronic and quark phases by minimization of the total energy including the surface and Coulomb contributions. In the Wigner-Seitz cell, the hadronic and quark phases are assumed to be separated by a sharp interface with a finite surface tension. The surface tension plays a crucial role in determining the structure of the mixed phase, but its value is poorly known. The calculation in the MIT bag model by using the multiple reflection expansion method [25] gave a value of the surface tension $\sigma \sim 10\,\mathrm{MeV}\,/\mathrm{fm}^2$, while a similar calculation in the

*shennankai@gmail.com

 ©2017 American Physical Society

Nambu-Jona-Lasinio (NJL) model including color superconductivity [26] yielded $\sigma \sim 145$–165 MeV/fm^2. The surface tension calculated from a geometrical approach fell in the range $\sigma \sim 7$–30 MeV/fm^2 [27]. Considering the uncertainty of σ, we treat the surface tension as a free parameter in the present study following the idea of Refs. [16,17,19]. Furthermore, the finite-size effects on the hadron-quark phase transition are examined by varying this parameter. The limit of $\sigma = 0$ corresponds to the absence of surface and Coulomb energies in the Gibbs construction.

The aim of the present work is to investigate the influence of surface and Coulomb contributions on the hadron-quark phase transition using the equilibrium conditions derived by minimization of the total energy. We employ the relativistic mean-field (RMF) model to describe the hadronic phase, while the NJL model is used for the quark phase. The NJL model can successfully describe dynamical chiral symmetry breaking and generation of constituent quark masses, so it has been widely used as an effective theory of QCD for the description of quark matter [9,28–31]. In this work, we adopt the three-flavor NJL model with a repulsive vector interaction. It has been extensively discussed in the literature that the inclusion of repulsive vector interactions could significantly affect the QCD phase diagram [32–34] and stiffen the equation of state (EOS) of quark matter which would result in larger maximum neutron-star masses [19,30,31,35–41]. For hadronic matter, we employ the RMF model with the parameter set TM1 [42], which can satisfactorily describe the properties of nuclear matter and finite nuclei. This model has been successfully applied to construct the EOS for supernova simulations and neutron stars [43,44]. With only nucleonic degrees of freedom, the TM1 model predicts a maximum neutron-star mass of 2.18 $M_\odot$. If Λ hyperons are allowed to appear, the maximum mass is reduced to 1.75 $M_\odot$ [44]. It is well known that the appearance of hyperons can significantly soften the EOS at high density and thus reduce the maximum neutron-star mass. The accurate mass determinations for PSR J1614-2230 [45,46] and PSR J0348+0432 [47] provide a strong constraint on the EOS of neutron-star matter. Most of the EOS including hyperons cannot satisfy the maximum mass constraint. It has been reported in Ref. [37] that by using the EOS interpolated between hadronic matter with hyperons and quark matter in a crossover region, the maximum neutron-star mass could be compatible with the observations, and an earlier onset of the hadron-quark crossover would provide a larger maximum mass. The authors of Ref. [37] considered several different hadronic EOSs obtained by G-matrix calculations and the chiral SU(3) symmetric RMF model, and they found that the qualitative conclusion is insensitive to the choice of the hadronic EOS. Currently there are large uncertainties in the contributions from hyperons at high density [48]. Therefore, we do not include hyperons in the present calculation and focus on the transition from nonstrange hadronic matter to deconfined quark matter with the inclusion of finite-size effects.

This article is organized as follows. In Sec. II, we briefly describe the RMF model for hadronic matter. In Sec. III, the NJL model used for quark matter is shortly introduced. In Sec. IV, we describe the hadron-quark mixed phase with finite-size effects and derive the equilibrium conditions for coexisting phases by minimization of the total energy including the surface and Coulomb contributions. In Sec. V, we present the numerical results and discuss the finite-size effects on the hadron-quark phase transition and neutron star properties. Section VI is devoted to the conclusions.

II. HADRONIC MATTER PHASE

We employ the RMF model to describe the hadronic matter phase. In the RMF approach, nucleons interact via the exchange of various mesons. The exchanged mesons considered here include the isoscalar scalar and vector mesons (σ and ω) and isovector vector meson ρ. We adopt the RMF model with the parameter set TM1, which provides an excellent description of nuclear matter and finite nuclei. For hadronic matter consisting of nucleons (p and n) and leptons (e and μ), the effective Lagrangian reads

$$\begin{aligned}\mathcal{L}_{\rm RMF} = &\sum_{i=p,n}\bar{\psi}_i(i\gamma_\mu\partial^\mu - M - g_\sigma\sigma - g_\omega\gamma_\mu\omega^\mu - g_\rho\gamma_\mu\tau_a\rho^{a\mu})\psi_i \\ &+ \frac{1}{2}\partial_\mu\sigma\partial^\mu\sigma - \frac{1}{2}m_\sigma^2\sigma^2 - \frac{1}{3}g_2\sigma^3 - \frac{1}{4}g_3\sigma^4 \\ &- \frac{1}{4}W_{\mu\nu}W^{\mu\nu} + \frac{1}{2}m_\omega^2\omega_\mu\omega^\mu + \frac{1}{4}c_3(\omega_\mu\omega^\mu)^2 \\ &- \frac{1}{4}R^a_{\mu\nu}R^{a\mu\nu} + \frac{1}{2}m_\rho^2\rho^a_\mu\rho^{a\mu} \\ &+ \sum_{l=e,\mu}\bar{\psi}_l(i\gamma_\mu\partial^\mu - m_l)\psi_l, \end{aligned} \tag{1}$$

where $W^{\mu\nu}$ and $R^{a\mu\nu}$ are the antisymmetric field tensors for ω^μ and $\rho^{a\mu}$, respectively. In the RMF approach, we treat the meson fields as classical fields and replace them by their expectation values. The nonvanishing expectation values of meson fields in hadronic matter are $\sigma = \langle\sigma\rangle$, $\omega = \langle\omega^0\rangle$, and $\rho = \langle\rho^{30}\rangle$. The equations of motion for the meson fields in uniform matter are given by

$$m_\sigma^2\sigma + g_2\sigma^2 + g_3\sigma^3 = -g_\sigma\left(n_p^s + n_n^s\right), \tag{2}$$

$$m_\omega^2\omega + c_3\omega^3 = g_\omega(n_p + n_n), \tag{3}$$

$$m_\rho^2\rho = g_\rho(n_p - n_n), \tag{4}$$

where n_i^s and n_i denote the scalar and number densities of species i, respectively. With the parameter set TM1 listed in Table I, these coupled equations are solved self-consistently, which yield that the nuclear matter saturation density is 0.145 fm^{-3}, the binding energy per nucleon is 16.3 MeV, the symmetry energy is 36.9 MeV, and the incompressibility is 281 MeV.

For hadronic matter in β equilibrium, the chemical potentials satisfy the relations $\mu_p = \mu_n - \mu_e$ and $\mu_\mu = \mu_e$. At zero temperature, the chemical potentials of leptons are expressed by $\mu_l = \sqrt{{k_F^l}^2 + m_l^2}$, while that of nucleons are given by $\mu_i = \sqrt{{k_F^i}^2 + M^{*2}} + g_\omega\omega + g_\rho\tau_3^i\rho$ with $M^* = M + g_\sigma\sigma$ being the effective nucleon mass. The total energy density of hadronic

TABLE I. Parameter set TM1 for the RMF Lagrangian. The masses are given in MeV.

Model	M	m_σ	m_ω	m_ρ	g_σ	g_ω	g_ρ	g_2 (fm^{-1})	g_3	c_3
TM1	938.0	511.198	783.0	770.0	10.0289	12.6139	4.6322	−7.2325	0.6183	71.3075

matter can be written as

$$\begin{aligned}\varepsilon_{\rm HP} &= \sum_{i=p,n}\frac{1}{\pi^2}\int_0^{k_F^i}\sqrt{k^2+M^{*2}}\,k^2dk+\frac{1}{2}m_\sigma^2\sigma^2+\frac{1}{3}g_2\sigma^3\\&+\frac{1}{4}g_3\sigma^4+\frac{1}{2}m_\omega^2\omega^2+\frac{3}{4}c_3\omega^4+\frac{1}{2}m_\rho^2\rho^2\\&+\sum_{l=e,\mu}\frac{1}{\pi^2}\int_0^{k_F^l}\sqrt{k^2+m_l^2}\,k^2dk,\end{aligned}\tag{5}$$

and the pressure is given by

$$\begin{aligned}P_{\rm HP} &= \sum_{i=p,n}\frac{1}{3\pi^2}\int_0^{k_F^i}\frac{k^4dk}{\sqrt{k^2+M^{*2}}}-\frac{1}{2}m_\sigma^2\sigma^2-\frac{1}{3}g_2\sigma^3\\&-\frac{1}{4}g_3\sigma^4+\frac{1}{2}m_\omega^2\omega^2+\frac{1}{4}c_3\omega^4+\frac{1}{2}m_\rho^2\rho^2\\&+\sum_{l=e,\mu}\frac{1}{3\pi^2}\int_0^{k_F^l}\frac{k^4dk}{\sqrt{k^2+m_l^2}}.\end{aligned}\tag{6}$$

III. QUARK MATTER PHASE

For the description of quark matter, we employ the NJL model with three flavors. The Lagrangian is written as

$$\begin{aligned}\mathcal{L}_{\rm NJL} &= \bar{q}(i\gamma_\mu\partial^\mu-m^0)q+G_S\sum_{a=0}^{8}[(\bar{q}\lambda_a q)^2+(\bar{q}i\gamma_5\lambda_a q)^2]\\&-K\{\det[\bar{q}(1+\gamma_5)q]+\det[\bar{q}(1-\gamma_5)q]\}\\&-G_V\sum_{a=0}^{8}[(\bar{q}\gamma^\mu\lambda_a q)^2+(\bar{q}\gamma^\mu\gamma_5\lambda_a q)^2],\end{aligned}\tag{7}$$

where q denotes the quark field with three flavors and three colors. The first term is the free Dirac Lagrangian with the current quark mass matrix given by $m^0=\mathrm{diag}(m_u^0,m_d^0,m_s^0)$. The second term with coupling G_S is a chirally symmetric four-quark interaction, where λ_a are the flavor SU(3) Gell-Mann matrices with $\lambda_0=\sqrt{2/3}\,I$. The third term corresponds to the six-quark Kobayashi–Maskawa–'t Hooft interaction that breaks the $U_A(1)$ symmetry. The last term introduces additional vector and axial-vector interactions with a positive coupling G_V that play important roles in describing massive stars [36–41]. In the present work, we adopt the parameters given in Ref. [49], $m_u^0=m_d^0=5.5$ MeV, $m_s^0=140.7$ MeV, $\Lambda=602.3$ MeV, $G_S\Lambda^2=1.835$, and $K\Lambda^5=12.36$. As for the vector coupling G_V, we treat it as a free parameter and take the ratios $G_V/G_S=0$, 0.2, and 0.4, in order to investigate the effect of the repulsive vector interaction on the equation of state.

In the NJL model at the mean-field level, the quarks get constituent quark masses by spontaneous chiral symmetry breaking. The constituent quark mass in vacuum m_i is considerably larger than the current quark mass m_i^0. In quark matter, the constituent quark masses m_i^* are determined from the coupled set of gap equations

$$m_i^*=m_i^0-4G_S\langle\bar{q}_iq_i\rangle+2K\langle\bar{q}_jq_j\rangle\langle\bar{q}_kq_k\rangle,\tag{8}$$

with (i,j,k) being any permutation of (u,d,s). $C_i=\langle\bar{q}_iq_i\rangle$ is the quark condensate of the flavor i. The energy density of quark matter is given by

$$\begin{aligned}\varepsilon_{\rm NJL} &= \sum_{i=u,d,s}\left[-\frac{3}{\pi^2}\int_{k_F^i}^{\Lambda}\sqrt{k^2+m_i^{*2}}\,k^2dk\right]\\&+2G_S\left(C_u^2+C_d^2+C_s^2\right)-4KC_uC_dC_s\\&+2G_V\left(n_u^2+n_d^2+n_s^2\right)-\varepsilon_0,\end{aligned}\tag{9}$$

where ε_0 is introduced to set $\varepsilon_{\rm NJL}=0$ in the physical vacuum. In Refs. [30,31], an effective bag constant B^* was introduced since there remains uncertainty in the low-density normalization of pressure in the NJL model. The authors of Ref. [31] varied the free parameter B^* in the range of -40 MeV/fm^3 to 50 MeV/fm^3, and they found that the hadron-quark transition density would increase with increasing B^*. In the present work, our choice of ε_0 corresponds to a vanishing pressure in the vacuum.

For the quark matter consisting of quarks (u, d, and s) and leptons (e and μ) in β equilibrium, the chemical potentials satisfy the relations $\mu_s=\mu_d=\mu_u+\mu_e$ and $\mu_\mu=\mu_e$. At zero temperature, the chemical potential of the quark flavor i is defined as $\mu_i=\sqrt{{k_F^i}^2+m_i^{*2}}+4G_V\,n_i$. The total energy density and pressure in the quark matter are given by

$$\varepsilon_{\rm QP}=\varepsilon_{\rm NJL}+\sum_{l=e,\mu}\frac{1}{\pi^2}\int_0^{k_F^l}\sqrt{k^2+m_l^2}\,k^2dk,\tag{10}$$

$$P_{\rm QP}=\sum_{i=u,d,s,e,\mu}n_i\mu_i-\varepsilon_{\rm QP}.\tag{11}$$

IV. HADRON-QUARK MIXED PHASE WITH FINITE-SIZE EFFECTS

To describe the hadron-quark mixed phase, we employ the Wigner-Seitz approximation, in which the system is divided into equivalent and charge-neutral cells. We assume that the coexisting hadronic and quark phases inside the cell are separated by a sharp interface and the leptons (electrons and muons) are uniformly distributed throughout the cell. It has been discussed that the geometrical structure of the mixed phase may change from droplet to rod, slab, tube, and bubble with increasing density [1,17]. For simplicity, we consider only droplet and bubble phases in the present study.

Generally, the surface and Coulomb contributions are neglected in the bulk approximation, where the mixed phase

is governed by the Gibbs conditions. When the finite-size effects are taken into account, the equilibrium conditions for coexisting hadronic and quark phases should be derived by minimization of the total energy including the surface and Coulomb contributions, which are different from the Gibbs conditions without finite-size effects. The total energy density of the hadron-quark mixed phase is written as

$$\varepsilon_{\rm MP} = u\varepsilon_{\rm QP} + (1-u)\varepsilon_{\rm HP} + \varepsilon_{\rm surf} + \varepsilon_{\rm Coul}, \tag{12}$$

where $u = V_{\rm QP}/(V_{\rm QP}+V_{\rm HP})$ is the volume fraction of the quark phase. The energy densities, $\varepsilon_{\rm HP}$ and $\varepsilon_{\rm QP}$, are given by Eqs. (5) and (10), respectively. The surface and Coulomb energy densities for a spherical cell are given by

$$\varepsilon_{\rm surf} = \frac{3\sigma u_{\rm in}}{r}, \tag{13}$$

$$\varepsilon_{\rm Coul} = \frac{e^2}{5}(\delta n_c)^2 r^2 u_{\rm in} D(u_{\rm in}), \tag{14}$$

where

$$D(u_{\rm in}) = 1 - \tfrac{3}{2}u_{\rm in}^{1/3} + \tfrac{1}{2}u_{\rm in}. \tag{15}$$

Here, $u_{\rm in}$ denotes the volume fraction of the inner part with radius r, i.e., $u_{\rm in} = u$ for droplets and $u_{\rm in} = 1-u$ for bubbles. σ is the surface tension of the hadron-quark interface, which is treated as a free parameter in the present calculation. $\delta n_c = n_c^{\rm HP} - n_c^{\rm QP}$ is the charge-density difference between the hadronic and quark phases. The energy density of the mixed phase $\varepsilon_{\rm MP}$ can be considered as a function of nine variables: $n_p, n_n, n_u, n_d, n_s, n_e, n_\mu, u$, and r. We derive the equilibrium conditions by minimizing $\varepsilon_{\rm MP}$ under the constraints of global charge neutrality and fixed average baryon density n_b, which are written as

$$0 = \frac{u}{3}(2n_u - n_d - n_s) + (1-u)n_p - n_e - n_\mu, \tag{16}$$

$$n_b = \frac{u}{3}(n_u + n_d + n_s) + (1-u)(n_p + n_n). \tag{17}$$

By introducing the Lagrange multipliers, μ_e and μ_n, for these two constraints, we perform the minimization for the function

$$w = \varepsilon_{\rm MP} - \mu_n\left[\frac{u}{3}(n_u + n_d + n_s) + (1-u)(n_p + n_n)\right] - \mu_e\left[n_e + n_\mu - \frac{u}{3}(2n_u - n_d - n_s) - (1-u)n_p\right]. \tag{18}$$

Minimizing w with respect to the particle densities yields the following equilibrium conditions for the chemical potentials:

$$\mu_u - \frac{4\varepsilon_{\rm Coul}}{3u\,\delta n_c} = \frac{1}{3}\mu_n - \frac{2}{3}\mu_e, \tag{19}$$

$$\mu_d + \frac{2\varepsilon_{\rm Coul}}{3u\,\delta n_c} = \frac{1}{3}\mu_n + \frac{1}{3}\mu_e, \tag{20}$$

$$\mu_s + \frac{2\varepsilon_{\rm Coul}}{3u\,\delta n_c} = \frac{1}{3}\mu_n + \frac{1}{3}\mu_e, \tag{21}$$

$$\mu_p + \frac{2\varepsilon_{\rm Coul}}{(1-u)\,\delta n_c} = \mu_n - \mu_e, \tag{22}$$

$$\mu_\mu = \mu_e. \tag{23}$$

The minimization over u leads to the equilibrium condition for the pressure

$$P_{\rm HP} = P_{\rm QP} - \frac{2\varepsilon_{\rm Coul}}{\delta n_c}\left[\frac{1}{3u}(2n_u - n_d - n_s) + \frac{1}{1-u}n_p\right] \mp \frac{\varepsilon_{\rm Coul}}{u_{\rm in}}\left(3 + u_{\rm in}\frac{D'}{D}\right), \tag{24}$$

where the sign of the last term is $-$ for droplets and $+$ for bubbles. The minimization over r results in the equilibrium condition between surface and Coulomb energies,

$$\varepsilon_{\rm surf} = 2\varepsilon_{\rm Coul}, \tag{25}$$

which implies that the radius of the droplet or bubble is given by

$$r = \left[\frac{15\sigma}{2e^2(\delta n_c)^2 D(u_{\rm in})}\right]^{1/3}. \tag{26}$$

It is clear that the equilibrium equations (19)–(24) are different from the Gibbs equilibrium conditions due to the inclusion of surface and Coulomb energies in the minimization procedure. However, these equations would reduce to the Gibbs conditions when the surface and Coulomb energies are neglected.

By solving the above equilibrium equations at a given baryon density n_b, we can obtain the properties of coexisting hadronic and quark phases, and then calculate thermodynamic quantities of the mixed phase. The pressure of the mixed phase is extracted from the thermodynamic relation, $P_{\rm MP} = n_b^2 \frac{\partial(\varepsilon_{\rm MP}/n_b)}{\partial n_b}$. Due to the inclusion of surface and Coulomb energies, $P_{\rm MP}$ is no longer equal to $P_{\rm HP}$ and $P_{\rm QP}$, which is similar to the case of nuclear liquid-gas phase transition at subnuclear densities [23,24,50].

V. RESULTS AND DISCUSSION

In this section, we present numerical results for the hadron-quark phase transition with finite-size effects. The hadron-quark mixed phase is obtained by solving the equilibrium conditions under the constraints of global charge neutrality and baryon number conservation. We consider both quark droplet and bubble phases in the Wigner-Seitz approximation. It has been pointed out in Ref. [16] that the droplet phase may become energetically unfavorable for large surface tension ($\sigma > 70\,{\rm MeV/fm^2}$), since the energy density of the droplet phase is higher than those of pure hadronic matter, pure quark matter, and the mixed phase in the Maxwell construction. In the present work, we first examine how large the surface tension is allowed to ensure that the droplet or bubble phase is energetically favorable. In Fig. 1, we plot the energy densities of the mixed phase for various values of the surface tension σ, relative to that of the Gibbs construction ($\sigma = 0$). The cross symbols mark the transition from the droplet phase to the bubble phase. The energy densities of pure hadronic matter and pure quark matter are shown for comparison. The mixed phase in the Maxwell construction, which contains locally charge-neutral hadronic and quark matter, has higher energy density than that of the Gibbs construction, and their differences are

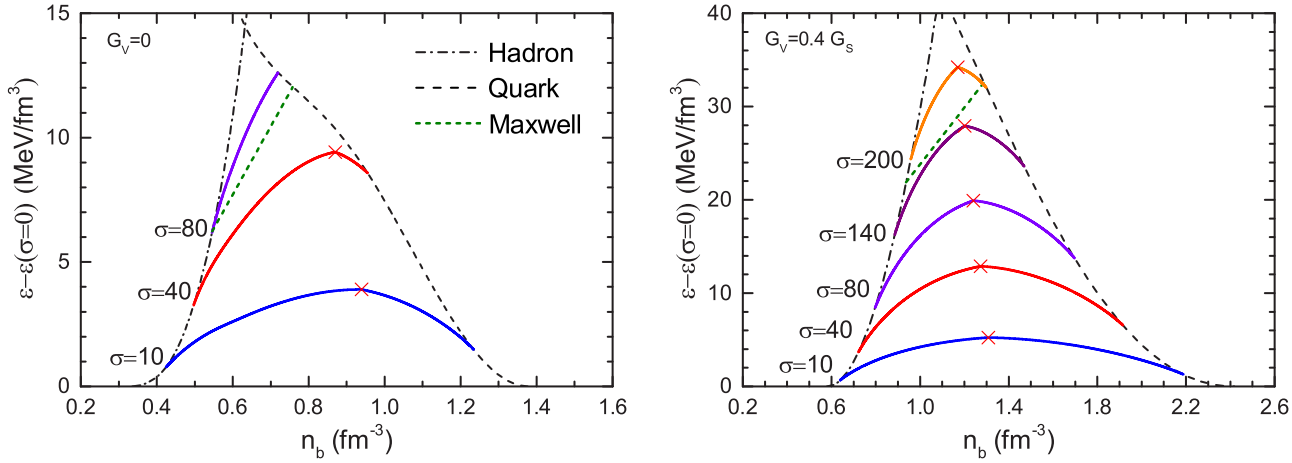

FIG. 1. Energy densities of the mixed phase for different values of the surface tension σ, relative to that of the Gibbs construction without surface and Coulomb energies ($\sigma = 0$). The cross symbols mark the transition from the droplet phase to the bubble phase. The results of the Maxwell construction are indicated by the green dotted lines. The left and right panels correspond to results for $G_V = 0$ and $G_V = 0.4\,G_S$, respectively.

indicated by the green dotted lines. The results with the vector coupling $G_V = 0$ and $G_V = 0.4\,G_S$ are displayed in the left and right panels, respectively. It is shown that the droplet or bubble phase with $\sigma > 80\,\mathrm{MeV/fm^2}$ ($\sigma > 200\,\mathrm{MeV/fm^2}$) for $G_V = 0$ ($G_V = 0.4\,G_S$) is energetically unfavorable due to its larger energy density than that of the Maxwell construction. This implies that the Maxwell construction is preferred and the local charge neutrality is required for such high surface tension. In this study, we focus on the difference from the Gibbs construction caused by surface and Coulomb energies, so we will perform the calculation for relatively small values of the surface tension. By comparing the left and right panels of Fig. 1, we can see that the density range of the mixed phase for $G_V = 0.4\,G_S$ is shifted to larger value and much wider than that for $G_V = 0$. This is because the repulsive vector interactions in the NJL model can significantly stiffen the EOS of quark matter, which results in a delay of the phase transition. At higher density, the surface tension has less impact on the mixed phase, and therefore the allowed values of the surface tension σ for $G_V = 0.4\,G_S$ are much larger than that for $G_V = 0$.

In Fig. 2, we show the density range of the mixed phase as a function of the surface tension σ for $G_V = 0$ (left panel) and $G_V = 0.4\,G_S$ (right panel). At the beginning of the mixed

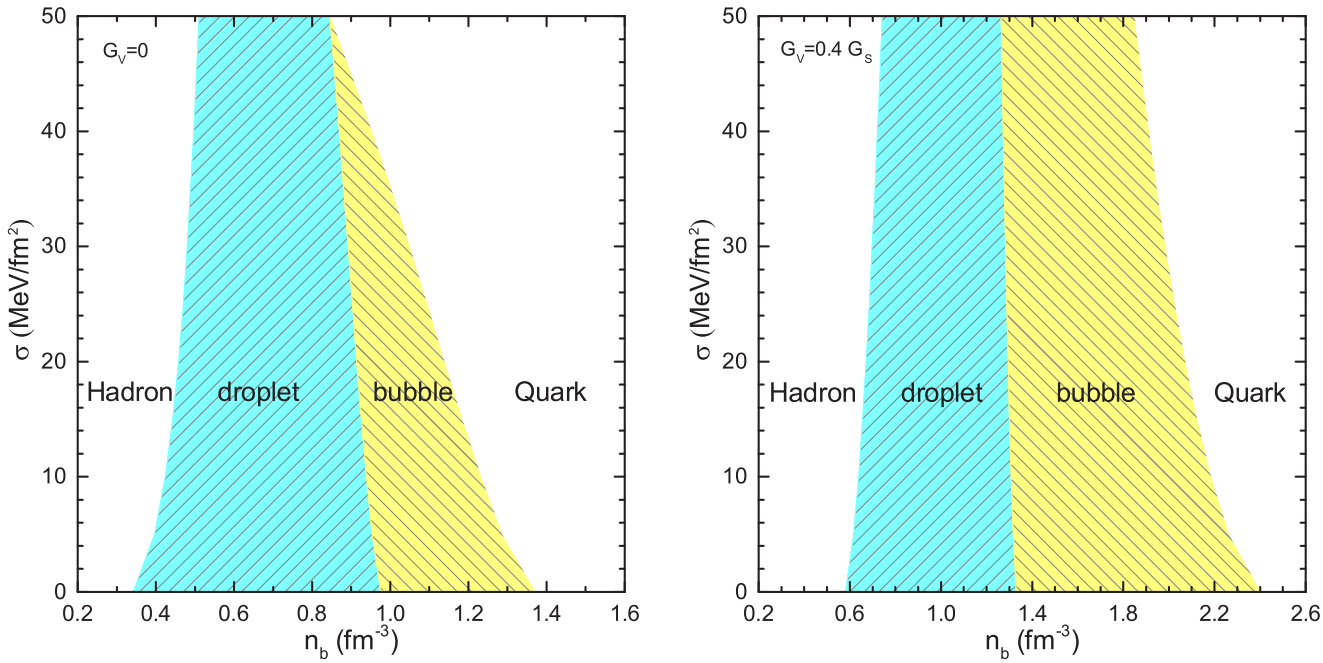

FIG. 2. Phase transition densities as a function of the surface tension σ. The shaded region indicates the density range of the mixed phase in the droplet and bubble configurations. The left and right panels correspond to results for $G_V = 0$ and $G_V = 0.4\,G_S$, respectively.

phase, quark matter occupies a small volume fraction and the favored structure is quark droplets embedded in hadronic matter. However, toward the end of the mixed phase, the quark bubble phase is more stable than the droplet phase. It is known that other geometrical structures, such as rod, slab, and tube, may exist in the middle of the mixed phase, which have been neglected in this calculation for simplicity. As one can see from Fig. 2, the density range of the mixed phase is significantly reduced as σ increases. Particularly, the range of the bubble phase gets smaller and eventually disappears for $\sigma > 50\,\mathrm{MeV/fm^2}$ in the case of $G_V = 0$. Compared to the left panel for $G_V = 0$, the density range of the mixed phase for $G_V = 0.4\,G_S$ (shown in the right panel) is shifted to higher densities and its dependence on σ is relatively weak. This is because, as density increases, the contribution from the surface term becomes less important relative to the bulk energy. As a result, the influence of the surface tension σ on the phase diagram becomes smaller at higher densities as shown in the right panel of Fig. 2.

It is interesting to examine the influence of surface and Coulomb energies on properties of the mixed phase. The Gibbs conditions for phase equilibrium demand equal pressures and chemical potentials for coexisting phases. However, when surface and Coulomb energies are taken into account, the pressure of quark matter is different from that of hadronic matter, as indicated in Eq. (24). In Fig. 3, we plot the pressures of hadronic and quark phases, $P_{\rm QP}$ and $P_{\rm HP}$, in the mixed phase obtained with $\sigma = 10$ and $40\ \mathrm{MeV/fm^2}$ for $G_V = 0$. It is shown that the differences between $P_{\rm QP}$ and $P_{\rm HP}$ are very small for $\sigma = 10\,\mathrm{MeV/fm^2}$, while evident differences are observed for $\sigma = 40\,\mathrm{MeV/fm^2}$, especially at low densities. The pressures coming from the surface and Coulomb energies

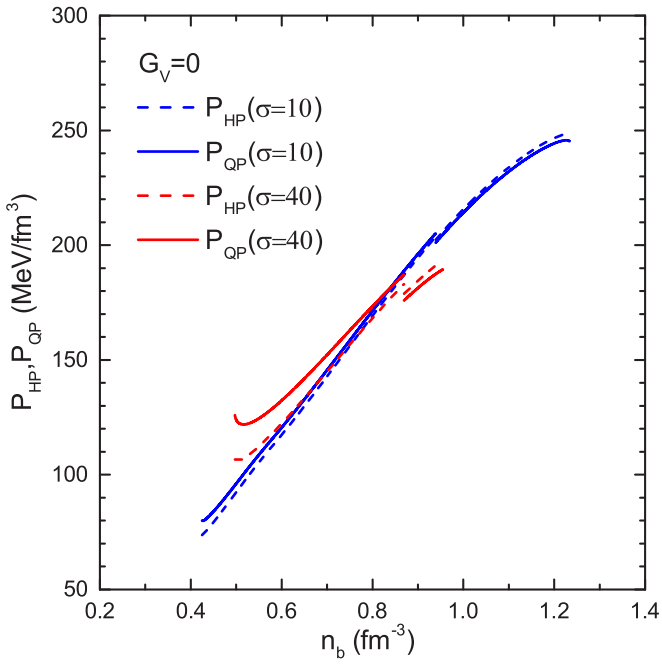

FIG. 3. Pressures of hadronic and quark phases, $P_{\rm HP}$ and $P_{\rm QP}$, as a function of the baryon density in the mixed phase with $\sigma = 10$ and $40\ \mathrm{MeV/fm^2}$ for $G_V = 0$.

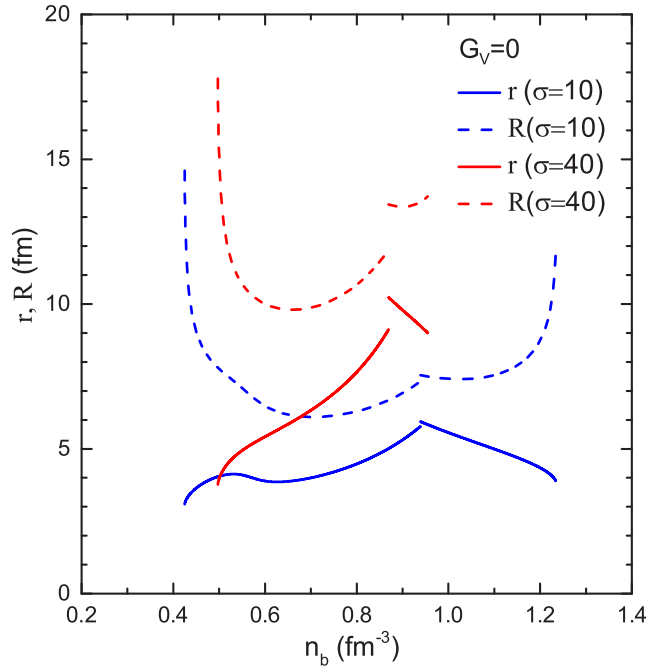

FIG. 4. Radius of the droplet or bubble (r) and that of the Wigner-Seitz cell (R) as a function of the baryon density with $\sigma = 10$ and $40\ \mathrm{MeV/fm^2}$ for $G_V = 0$.

have opposite signs, and the one from the surface tension is somewhat larger than that from the Coulomb energy. Therefore, the pressure of the inner phase is slightly higher than that outside. In Fig. 4, we show the radius of the inner part (r) and that of the Wigner-Seitz cell (R) as a function of the baryon density n_b obtained with $\sigma = 10$ and $40\,\mathrm{MeV/fm^2}$ for $G_V = 0$. As density increases, we can see that r increases in the droplet phase and then turns to decrease in the bubble phase, but R shows rather different behavior. This is related to the increase of the quark volume fraction in the mixed phase. It is seen that both r and R for $\sigma = 40\,\mathrm{MeV/fm^2}$ are larger than those for $\sigma = 10\,\mathrm{MeV/fm^2}$. This is because a large value of σ favors a large r as indicated in Eq. (26), and meanwhile, a large R is achieved according to $R = r u_{\rm in}^{-1/3}$. In Fig. 5, the electric charge densities of hadronic and quark phases, $n_c^{\rm HP}$ and $n_c^{\rm QP}$, are shown as a function of n_b for the same values of σ and G_V as in Figs. 3 and 4. The Gibbs construction corresponds to $\sigma = 0$, which contains positively charged hadronic matter and negatively charged quark matter with relatively large differences between $n_c^{\rm HP}$ and $n_c^{\rm QP}$. In contrast, the Maxwell construction consists of two charge-neutral phases, i.e., $n_c^{\rm HP} = n_c^{\rm QP} = 0$, which is caused by extremely high surface tension. The results obtained with $\sigma = 10$ and $40\ \mathrm{MeV/fm^2}$ are somewhat different from those of the Gibbs construction, and a larger value of σ results in more significant differences. In Figs. 3–5, we show results only for $G_V = 0$; however, similar behaviors are observed for other values of G_V.

In Fig. 6, we plot the pressures as a function of the baryon density for hadronic, mixed, and quark phases. The left, middle, and right panels show respectively the results for $G_V = 0$, $0.2\,G_S$, and $0.4\,G_S$, while the upper and lower

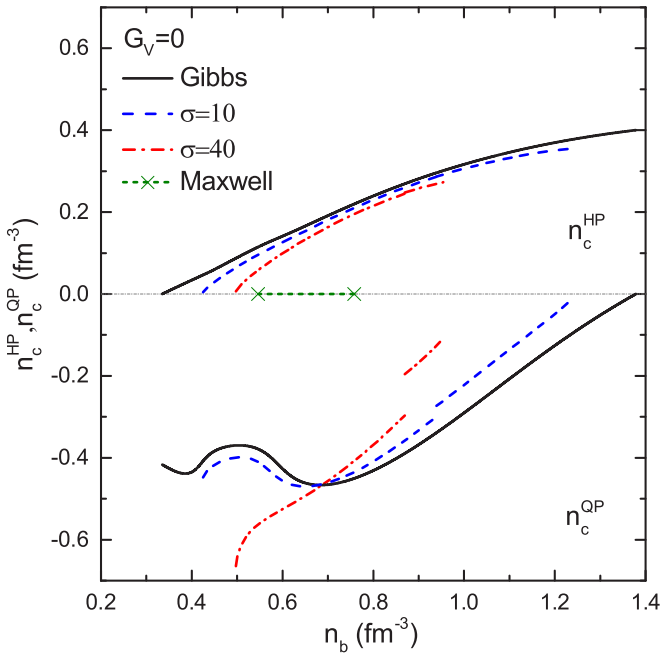

FIG. 5. Charge densities of hadronic and quark phases, $n_c^{\rm HP}$ and $n_c^{\rm QP}$, as a function of the baryon density. The results with $\sigma = 10$ and 40 MeV/fm^2 are compared to those of the Gibbs and Maxwell constructions.

panels correspond to the results of the mixed phase obtained with $\sigma = 10$ and 40 MeV/fm^2. The droplet and bubble phases are indicated by the red and purple solid lines. For comparison, results with the Gibbs and Maxwell constructions are shown by the blue dashed and green dotted lines, respectively. It is shown that pressures of the mixed phase obtained with a finite value of σ lie between those of the Gibbs and Maxwell constructions. The results of $\sigma = 10\,{\rm MeV/fm}^2$ (upper panels) are closer to that of the Gibbs construction than those of $\sigma = 40\,{\rm MeV/fm}^2$ (lower panels). By comparing the left, middle, and right panels, one can see the effect of the repulsive vector interactions in the NJL model. As the vector coupling G_V increases, the EOS of quark matter gets stiffer. As a result, the mixed phase exists in a broad density range and moves toward higher densities.

To examine the finite-size effects on properties of neutron stars, we solve the Tolman-Oppenheimer-Volkoff equation by using the EOS described above for $G_V = 0$ (left panel) and $G_V = 0.4\,G_S$ (right panel). For the description of neutron-star crusts, the present EOS is matched to the EOS at subnuclear densities, which was calculated from the Thomas-Fermi approximation by using the TM1 model for nuclear interactions [43]. The resulting mass-radius relations are presented in Fig. 7, where the observational constraints of PSR J0348-0432 ($M = 2.01 \pm 0.04\,M_\odot$) [47] and PSR J1614-2230 ($M = 1.928 \pm 0.017\,M_\odot$) [46] are shown by the lighter and darker shaded regions, respectively. For comparison, results of pure hadronic EOS are shown by thin solid lines, which give a maximum mass of 2.18 $M_\odot$ [44]. The inclusion of quark degrees of freedom significantly softens the EOS and reduces the maximum mass of neutron stars, which depends on the vector coupling G_V, as shown in the two panels of Fig. 7. In the case of $G_V = 0.4\,G_S$ ($G_V = 0$), the maximum mass with the Gibbs construction is reduced to 2.13 $M_\odot$ (1.91 $M_\odot$). When the finite-size effects are taken into account, neutron-star masses are somewhat higher than those of the Gibbs construction and the differences depend on the surface tension σ. In Table II, the calculated properties of neutron stars with the maximum mass are presented in detail. For the cases of

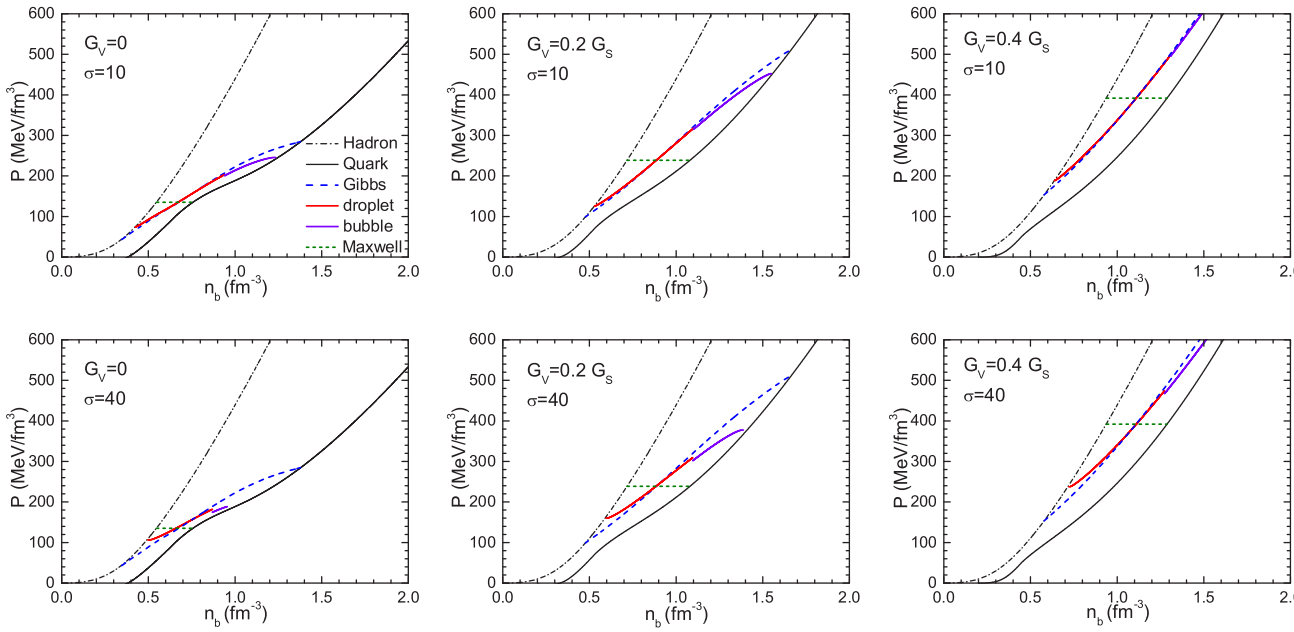

FIG. 6. Pressures as a function of the baryon density for hadronic, mixed, and quark phases. The results of the mixed phase with $\sigma = 10\,{\rm MeV/fm}^2$ (upper panel) and $\sigma = 40\,{\rm MeV/fm}^2$ (lower panel) are compared to those of the Gibbs and Maxwell constructions. The results for $G_V = 0$, $G_V = 0.2\,G_S$, and $G_V = 0.4\,G_S$ are shown in the left, middle, and right panels, respectively.

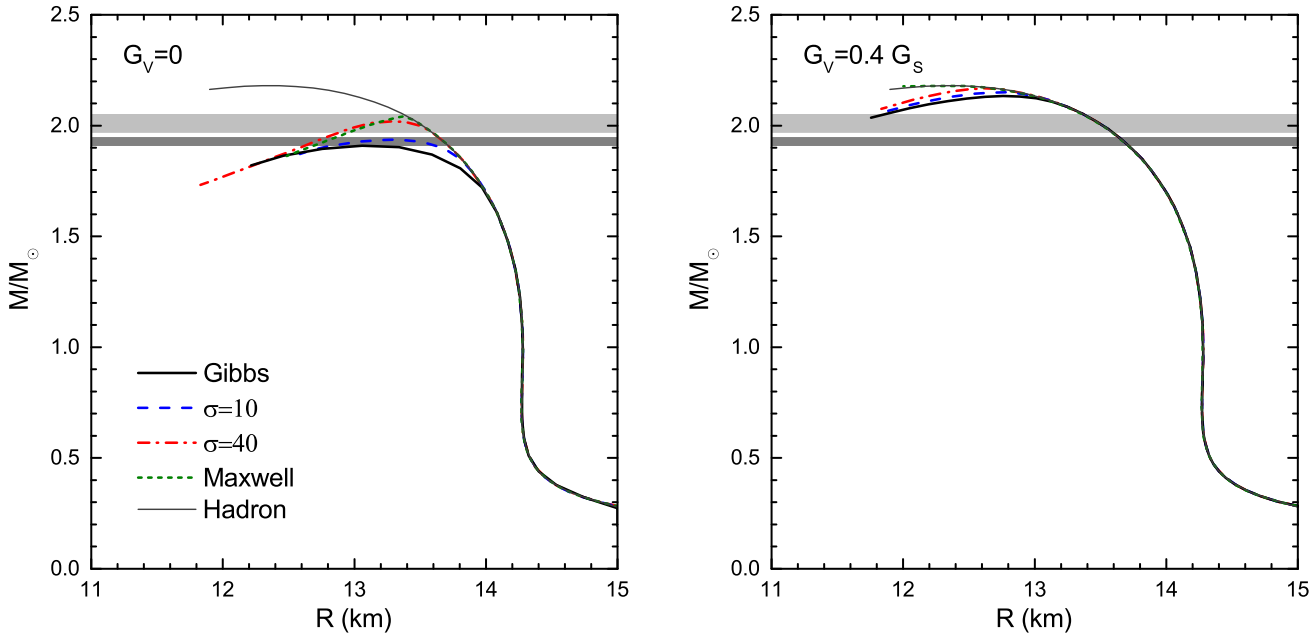

FIG. 7. Mass-radius relations of neutron stars for different EOS. For comparison, the results from a pure hadronic EOS are shown by the thin solid lines. The lighter and darker shaded regions correspond to the observational constraints of PSR J0348-0432 ($M = 2.01 \pm 0.04\ M_\odot$) [47] and PSR J1614-2230 ($M = 1.928 \pm 0.017\ M_\odot$) [46], respectively.

$\sigma = 0$ (Gibbs), 10, and 40 MeV/fm^2, a mixed-phase core with radius $R_{\rm MP}$ can be formed in the interior of stars and $R_{\rm MP}$ decreases with increasing G_V, but the central density is not high enough to generate pure quark matter. For the Maxwell construction, the mixed phase is not allowed to appear in stars because of its constant pressure. However, a small quark phase core may exist with $R_{\rm QP} = 0.82$ km for $G_V = 0$ and $R_{\rm QP} = 0.38$ km for $G_V = 0.2\,G_S$. We notice that there is no quark matter in the interior of neutron stars for larger vector coupling $G_V = 0.4\,G_S$, as shown in the last line of Table II. It is found that the internal structures of neutron stars are rather sensitive to the values of the surface tension σ and the vector coupling G_V.

VI. CONCLUSIONS

We have investigated the finite-size effects on the hadron-quark phase transition, which may occur in the interior of massive neutron stars. The RMF model has been used to describe the hadronic matter phase, while the NJL model with vector interactions has been adopted for the quark matter phase. We have employed the Wigner-Seitz approximation to describe the hadron-quark mixed phase, where the coexisting hadronic and quark phases inside the charge-neutral cell are separated by a sharp interface. We have derived the equilibrium conditions for coexisting hadronic and quark phases by minimization of the total energy including the surface and Coulomb contributions. It has been found that

TABLE II. Properties of neutron stars with the maximum mass $M_{\rm max}$. The central energy density and baryon number density are denoted by ε_c and n_c, respectively. $R_{\rm QP}$, $R_{\rm MP}$, and R correspond to radii of the quark phase, the mixed phase, and the whole star.

		$M_{\rm max}$ ($M_\odot$)	ε_c (MeV/fm^3)	n_c (fm^{-3})	$R_{\rm QP}$ (km)	$R_{\rm MP}$ (km)	R (km)
Gibbs	$G_V = 0$	1.91	876.3	0.76		7.80	13.09
	$G_V = 0.2\,G_S$	2.05	912.4	0.77		5.60	13.00
	$G_V = 0.4\,G_S$	2.13	963.9	0.80		4.50	12.77
$\sigma = 10$ MeV/fm^2	$G_V = 0$	1.94	798.2	0.70		5.60	13.30
	$G_V = 0.2\,G_S$	2.08	907.3	0.77		4.50	13.01
	$G_V = 0.4\,G_S$	2.15	948.7	0.79		3.41	12.77
$\sigma = 40$ MeV/fm^2	$G_V = 0$	2.00	792.4	0.69		3.64	13.37
	$G_V = 0.2\,G_S$	2.11	889.0	0.75		2.95	13.03
	$G_V = 0.4\,G_S$	2.17	981.5	0.81		2.26	12.67
Maxwell	$G_V = 0$	2.04	896.1	0.77	0.82		13.40
	$G_V = 0.2\,G_S$	2.16	1395.3	1.08	0.38		12.77
	$G_V = 0.4\,G_S$	2.18	1081.2	0.87			12.30

these equilibrium conditions are different from the Gibbs conditions used in the bulk calculations due to the inclusion of surface and Coulomb energies. As a consequence, the pressure of quark matter is no longer equal to that of hadronic matter, and the differences are more pronounced for larger values of the surface tension.

The effects of the surface tension σ and the vector coupling G_V on properties of the hadron-quark mixed phase have been investigated in the present work. For large values of σ, the density range of the mixed phase is significantly reduced with respect to that of the Gibbs construction. Furthermore, a larger surface tension generally leads to a larger structure size and smaller charge density difference between the two phases. Since the Gibbs and Maxwell constructions correspond, respectively, to the two limits of zero and infinite surface tension, results for finite values of the surface tension were found to lie between these two limits. The repulsive vector interactions in the NJL model could stiffen the EOS of quark matter, and as a result, the mixed phase would exist in a broad density range and move toward higher densities.

The properties of neutron stars have been calculated with the inclusion of finite-size effects. The maximum masses of neutron stars were found to depend on both the surface tension σ and the vector coupling G_V, which increase with increasing σ and G_V. The maximum masses for finite values of σ were found to lie between results of the Gibbs and Maxwell constructions. A mixed-phase core might be formed in the interior of massive stars, but no pure quark phase could exist for relatively small surface tension in the present study. In the case of the Maxwell construction, a small pure quark core could appear for smaller values of G_V. It has been noticed that our results of neutron stars could be compatible with the observations of PSR J1614-2230 and PSR J0348-0432. Finally, we emphasize that the surface tension of the hadron-quark interface and the vector interaction between quarks play critical roles in determining behaviors of the hadron-quark phase transition and neutron star properties. Therefore, better estimates for these quantities are needed for further studies.

ACKNOWLEDGMENT

This work was supported in part by the National Natural Science Foundation of China (Grants No. 11375089 and No. 11675083).

[1] N. K. Glendenning, Phys. Rep. **342**, 393 (2001).
[2] H. Heiselberg and M. Hjorth-Jensen, Phys. Rep. **328**, 237 (2000).
[3] F. Weber, Prog. Part. Nucl. Phys. **54**, 193 (2005).
[4] N. K. Glendenning, Phys. Rev. D **46**, 1274 (1992).
[5] K. Schertler, S. Leupold, and J. Schaffner-Bielich, Phys. Rev. C **60**, 025801 (1999).
[6] K. Schertler, C. Greiner, J. Schaffner-Bielich, and M. H. Thoma, Nucl. Phys. A **677**, 463 (2000).
[7] A. W. Steiner, M. Prakash, and J. M. Lattimer, Phys. Lett. B **486**, 239 (2000).
[8] G. F. Burgio, M. Baldo, P. K. Sahu, and H.-J. Schulze, Phys. Rev. C **66**, 025802 (2002).
[9] D. P. Menezes and C. Providência, Phys. Rev. C **68**, 035804 (2003).
[10] B. K. Sharma, P. K. Panda, and S. K. Patra, Phys. Rev. C **75**, 035808 (2007).
[11] F. Yang and H. Shen, Phys. Rev. C **77**, 025801 (2008).
[12] J. Xu, L. W. Chen, C. M. Ko, and B. A. Li, Phys. Rev. C **81**, 055803 (2010).
[13] H. Chen, G. F. Burgio, H.-J. Schulze, and N. Yasutake, Astron. Astrophys. **551**, A13 (2013).
[14] M. Orsaria, H. Rodrigues, F. Weber, and G. A. Contrera, Phys. Rev. C **89**, 015806 (2014).
[15] A. Bhattacharyya, I. N. Mishustin, and W. Greiner, J. Phys. G **37**, 025201 (2010).
[16] H. Heiselberg, C. J. Pethick, and E. F. Staubo, Phys. Rev. Lett. **70**, 1355 (1993).
[17] T. Endo, T. Maruyama, S. Chiba, and T. Tatsumi, Prog. Theor. Phys. **115**, 337 (2006).
[18] T. Maruyama, S. Chiba, H.-J. Schulze, and T. Tatsumi, Phys. Rev. D **76**, 123015 (2007).
[19] N. Yasutake, R. Łastowiecki, S. Benić, D. Blaschke, T. Maruyama, and T. Tatsumi, Phys. Rev. C **89**, 065803 (2014).
[20] N. K. Glendenning and S. Pei, Phys. Rev. C **52**, 2250 (1995).
[21] M. B. Christiansen and N. K. Glendenning, Phys. Rev. C **56**, 2858 (1997).
[22] D. N. Voskresensky, M. Yasuhira, and T. Tatsumi, Nucl. Phys. A **723**, 291 (2005).
[23] J. M. Lattimer and F. D. Swesty, Nucl. Phys. A **535**, 331 (1991).
[24] S. S. Bao, J. N. Hu, Z. W. Zhang, and H. Shen, Phys. Rev. C **90**, 045802 (2014).
[25] M. S. Berger and R. L. Jaffe, Phys. Rev. C **35**, 213 (1987); **44**, 566(E) (1991).
[26] G. Lugones, A. G. Grunfeld, and M. A. Ajmi, Phys. Rev. C **88**, 045803 (2013).
[27] M. B. Pinto, V. Koch, and J. Randrup, Phys. Rev. C **86**, 025203 (2012).
[28] T. Hatsuda and T. Kunihiro, Phys. Rep. **247**, 221 (1994).
[29] M. Buballa, Phys. Rep. **407**, 205 (2005).
[30] D. Logoteta, C. Providência, and I. Vidaña, Phys. Rev. C **88**, 055802 (2013).
[31] L. Bonanno and A. Sedrakian, Astron. Astrophys. **539**, A16 (2012).
[32] K. Fukushima, Phys. Rev. D **77**, 114028 (2008); **78**, 039902(E) (2008).
[33] H. Ueda, T. Z. Nakano, A. Ohnishi, M. Ruggieri, and K. Sumiyoshi, Phys. Rev. D **88**, 074006 (2013).
[34] M. Buballa and S. Carignano, Prog. Part. Nucl. Phys. **81**, 39 (2015).
[35] G. Pagliara and J. Schaffner-Bielich, Phys. Rev. D **77**, 063004 (2008).
[36] H. Abuki, R. Gatto, and M. Ruggieri, Phys. Rev. D **80**, 074019 (2009).
[37] K. Masuda, T. Hatsuda, and T. Takatsuka, Astrophys. J. **764**, 12 (2013); Prog. Theor. Exp. Phys. **2013**, 073D01 (2013).
[38] D. P. Menezes, M. B. Pinto, L. B. Castro, P. Costa, and C. Providência, Phys. Rev. C **89**, 055207 (2014).

[39] T. Hell and W. Weise, Phys. Rev. C **90**, 045801 (2014).
[40] P. C. Chu, X. Wang, L. W. Chen, and M. Huang, Phys. Rev. D **91**, 023003 (2015).
[41] R. C. Pereira, P. Costa, and C. Providência, Phys. Rev. D **94**, 094001 (2016).
[42] Y. Sugahara and H. Toki, Nucl. Phys. A **579**, 557 (1994).
[43] H. Shen, Phys. Rev. C **65**, 035802 (2002).
[44] H. Shen, H. Toki, K. Oyamatsu, and K. Sumiyoshi, Astrophys. J. Suppl. **197**, 20 (2011).
[45] P. B. Demorest, T. Pennucci, S. M. Ranson, M. S. E. Roberts, and J. W. T. Hessels, Nature (London) **467**, 1081 (2010).
[46] E. Fonseca, T. T. Pennucci, J. A. Ellis, I. H. Stairs, D. J. Nice, S. M. Ransom, P. B. Demorest, Z. Arzoumanian, K. Crowter, T. Dolch *et al.*, Astrophys. J. **832**, 167 (2016).
[47] J. Antoniadis, P. C. C. Freire, N. Wex, T. M. Tauris, R. S. Lynch, M. H. van Kerkwijk, M. Kramer, C. Bassa, V. S. Dhillon, T. Driebe *et al.*, Science **340**, 1233232 (2013).
[48] S. Weissenborn, D. Chatterjee, and J. Schaffner-Bielich, Nucl. Phys. A **881**, 62 (2012).
[49] P. Rehberg, S. P. Klevansky, and J. Hüfner, Phys. Rev. C **53**, 410 (1996).
[50] G. Baym, H. A. Bethe, and C. J. Pethick, Nucl. Phys. A **175**, 225 (1971).